Atmos. Chem. Phys. Discuss., doi:10.5194/acp-2016-160, 2016
Manuscript under review for journal Atmos. Chem. Phys.
Published: 11 March 2016

Atmospheric Chemistry and Physics Discussions
Open Access

Global tropospheric hydroxyl distribution, budget and reactivity

J. Lelieveld[1], S. Gromov[1], A. Pozzer[1], and D. Taraborrelli[1]

[1]Max Planck Institute for Chemistry, P.O. Box 3060, 55020 Mainz, Germany

Correspondence to: J. Lelieveld (jos.lelieveld@mpic.de)

Abstract. The self-cleaning or oxidation capacity of the atmosphere is principally controlled by hydroxyl (OH) radicals in the troposphere. Hydroxyl has primary (*P*) and secondary (*S*) sources, the former through the photo-dissociation of ozone, the latter through OH recycling in radical reaction chains. We used the recent Mainz Organics Mechanism (MOM) to advance volatile organic carbon (VOC) chemistry in the general circulation model EMAC, and show that *S* is larger than previously assumed. MOM calculates substantially higher OH reactivity from VOC oxidation compared to predecessor models. Further, we find that nighttime OH formation may be significant in the polluted subtropical boundary layer in summer. Globally *S* exceeds *P*, most distinctively in the free troposphere. As a consequence, OH is buffered and not sensitive to perturbations by natural or anthropogenic emission changes. Complementary OH formation mechanisms in pristine and polluted environments of the continental and marine troposphere, connected through long-range transport of O_3, maintain stable global OH levels.

1 Introduction

The removal of most natural and anthropogenic gases from the atmosphere, important for air quality, the ozone layer and climate, takes place through their oxidation by hydroxyl (OH) radicals in the troposphere. The central role of tropospheric OH in the atmospheric oxidation capacity (or efficiency) has been recognized since the early 1970s (Levy, 1971; Crutzen, 1973; Logan et al., 1981, Ehhalt et al., 1991). The primary OH formation rate (*P*) depends on the photo-dissociation of ozone (O_3) by ultraviolet (UV) sunlight – with a wavelength of the photon ($h\nu$) shorter than 330 nm – in the presence of water vapor

$$O_3 + h\nu\ (\lambda<330\ \text{nm}) \rightarrow O(^1D) + O_2 \quad \text{(R1)}$$

$$O(^1D) + H_2O \rightarrow 2OH \quad \text{(R2)}$$

The ozone layer in the tropics is relatively thin, hence UV radiation is less strongly attenuated compared to the extra-tropics, and also because the solar zenith angle and water vapor concentrations are relatively high, zonal OH is highest at low latitudes in the lower to middle troposphere (Crutzen and Zimmermann, 1991; Spivakowski et al., 2000).

The OH radicals attack reduced and partly oxidized gases such as methane (CH_4), non-methane volatile organic compounds (VOCs) and carbon monoxide (CO), so that these gases only occur in trace amounts, e.g.,

$$CO + OH \rightarrow CO_2 + H \quad \text{(R3)}$$

Atmos. Chem. Phys. Discuss., doi:10.5194/acp-2016-160, 2016
Manuscript under review for journal Atmos. Chem. Phys.
Published: 11 March 2016

Atmospheric Chemistry and Physics
Discussions

$H + O_2\ (+M) \rightarrow HO_2\ (+M)$ (R4)

where M is an air molecule that removes excess energy from the reaction. As OH is highly reactive it has an average tropospheric lifetime of about 1-2 seconds. After the initial OH reaction (R3) peroxy radicals are produced (R4), which can recombine to form peroxides

$HO_2 + HO_2 \rightarrow H_2O_2 + O_2$ (R5)

$RO_2 + HO_2 \rightarrow ROOH + O_2$ (R6)

RH is a VOC that produces a radical R upon H-extraction by OH, e.g., an alkyl radical, that reacts with O_2 to form RO_2. After formation of a peroxide the reaction chains can either propagate or terminate, the latter by deposition. Propagation of the chain leads to higher generation reaction products and secondary OH formation (*S*), which can be understood as OH recycling. For example, the photolysis of ROOH leads to OH production. In air that is directly influenced by pollution emissions *S* is largely controlled by nitrogen oxides ($NO+NO_2=NO_X$)

$NO + HO_2 \rightarrow NO_2 + OH$ (R7)

This leads to ozone production through photo-dissociation of NO_2 by ultraviolet and visible light

$NO_2 + h\nu\ (\lambda<430nm) \rightarrow NO + O(^3P)$ (R8)

$O(^3P) + O_2\ (+M) \rightarrow O_3\ (+M)$ (R9)

However, in strongly polluted air NO_2 can also be a dominant OH sink, hence the net effect of NO_X on OH is self-limiting

$NO_2 + OH\ (+M) \rightarrow HNO_3\ (+M)$ (R10)

Conversely, under low-NO_X conditions, mostly in pristine air, secondary OH formation by other mechanisms is important

$O_3 + HO_2 \rightarrow 2O_2 + OH$ (R11)

$H_2O_2 + h\nu\ (\lambda<550\ nm) \rightarrow OH + OH$ (R12)

In prior work we suggested that the strong growth of air pollution since industrialization, especially in the 20th century, has drastically changed OH production and loss rates, but that globally the balance between *P* and *S* changed little (Lelieveld et al., 2002). This is associated with a relatively constant OH recycling probability *r*, defined as $r = 1 - P/G$, in which *G* is gross OH formation (*P*+*S*). Thus, in the past century *G* (the atmospheric oxidation power) kept pace with the growing OH sink related to the emissions of reduced and partly oxidized pollution gases.

While globally *r* has remained approximately constant, the mean tropospheric OH concentration and the lifetime of CH_4 (τ_{CH4}) have also changed comparatively little, for example within a spread of about 15% calculated by a 17-member ensemble of atmospheric chemistry-transport models (Naik et al., 2013). Despite substantial differences in OH concentrations and τ_{CH4} among the models, simulations of emission scenarios according to several Representative Concentration Pathways indicate that future OH changes will probably also be small, i.e., well within 10% (Voulgarakis et al., 2013). We interpret the relative constancy of *r*, mean OH and τ_{CH4} as indication that global OH is buffered against perturbations. This is corroborated by observation-based studies, showing small inter-annual variability of global OH and a small inter-hemispheric difference in OH (Krol and Lelieveld, 2003; Montzka et al., 2011; Patra et al., 2014).

Atmos. Chem. Phys. Discuss., doi:10.5194/acp-2016-160, 2016
Manuscript under review for journal Atmos. Chem. Phys.
Published: 11 March 2016

Atmospheric Chemistry and Physics
Discussions

In our previous estimates of *P* and *S* we used a chemistry-transport model with the Carbon Bond Mechanism (CBM) to represent non-hydrocarbon chemistry (Houweling et al., 1998). This mechanism aggregates organic compounds into categories of species according to molecular groups, and has been successfully used to simulate ozone concentrations with air quality models (Stockwell et al., 2012). However, such chemical schemes are not mass-conserving, e.g., for carbon, and are optimized for conditions in which NO_X dominates *r*, while in low-NO_X environments other mechanisms may be important, for example through the chemistry of non-methane VOCs emitted by vegetation (Lelieveld et al., 2008), as reviewed by Vereecken and Francisco (2012), Stone et al. (2012) and Monks et al. (2015). A limitation of the CBM and other, similar mechanisms is that 2nd and higher generation reaction products are lumped or ignored for computational efficiency, whereas they can contribute importantly to OH recycling and ozone chemistry (Butler et al., 2011; Taraborrelli et al., 2012).

Here we apply the Mainz Organics Mechanism (MOM) that accounts for recent developments in atmospheric VOC chemistry (Taraborrelli et al., manuscript in preparation). The MOM is a further development of the Mainz Isoprene Mechanism (Taraborrelli et al., 2009). In addition to isoprene, MOM computes the chemistry of saturated and unsaturated hydrocarbons, including terpenes and aromatics. Based on this scheme, implemented in the atmospheric chemistry – general circulation model EMAC, we provide an update of global OH calculations, sources, sinks, tropospheric distributions, OH reactivity, the lifetime of CH_4 and CO, and discuss implications for atmospheric chemistry. We contrast the boundary layer and free troposphere (BL and FT), the Northern and Southern Hemisphere (NH and SH) and the tropics and extra-tropics. We show that complementary OH recycling mechanisms in terrestrial, marine, pristine and polluted environments, inter-connected through atmospheric transport, sustain stable levels of hydroxyl in the global troposphere.

2 VOC chemistry and model description

To reconcile observations of high OH concentrations over the Amazon rainforest with models that predicted low OH concentrations, we have proposed that the chemistry of isoprene recycles OH, e.g., involving organic peroxy radicals (Lelieveld et al., 2008). Progress on such reactions was reported by Taraborelli et al. (2012) and incorporated in a predecessor version of the present chemistry scheme. Laboratory experimental results by Groß et al. (2014a,b) provided additional evidence and insight into this type of chemistry, indicating that OH formation via reaction R6 (RO_2+HO_2) had previously been underestimated significantly. While in polluted air peroxy radicals preferentially react with NO, in pristine, low-NO_X conditions over the rain forest, e.g., in the Amazon, isoprene degradation leads to hydroxy-hydroperoxides, which can reform OH upon further oxidation (Paulot et al., 2009).

An important pathway that can recycle OH is isomerization through H-migration within oxygenated isoprene reaction products, leading to photo-labile hydroperoxy-aldehydes (HPALD), as reviewed by Vereecken and Francisco (2012). While a high rate of 1,5-H-shifts that we have assumed previously (Taraborrelli et al., 2012) was not confirmed experimentally, these and especially 1,4-H- and 1,6-H-shifts have nevertheless shown to be key intermediaries in OH recycling (Crounse et al., 2012, 2013; Fuchs et al., 2014; Peeters et al., 2014). Next to HPALD, unsaturated hydroperoxyaldehydes, e.g., peroxyacylaldehydes (PACALD), were shown to be relevant (Peeters et al., 2014). Higher generation reaction products include several organic peroxides that produce OH upon photo-dissociation, which need to be accounted for in atmospheric chemistry models to reproduce field and reaction chamber observations (Nölscher et al., 2014).

These reactions have been included into the Mainz Organics Mechanism (MOM), being an extension and update of the Mainz Isoprene Mechanism, v.2 (Taraborrelli et al., 2009). The scheme, which accounts for about 630 compounds and 1630 reactions, makes use of rate constant estimation methods similarly to and in some cases like the Master Chemical Mechanism by Jenkin et al. (2015) (http://mcm.leeds.ac.uk/MCM), and recommendations by the Task Group on Atmospheric Chemical Kinetic Data Evaluation (http://iupac.pole-ether.fr), in addition to our own evaluation of recent literature. For computational efficiency in global and regional models, the scheme will be condensed into several hundred reactions in future (Taraborrelli et al., in preparation). In contrast to many previous chemistry mechanisms in atmospheric models, MOM accounts for higher generation reaction products and is mass conserving (notably carbon containing reaction products from VOC oxidation).

The MOM has been included into the ECHAM/MESSy Atmospheric Chemistry (EMAC) general circulation model. The core atmospheric general circulation model is ECHAM5 (Roeckner et al., 2006), interconnected with the Modular Earth Submodel System (MESSy v.2; Jöckel et al., 2005, 2010). EMAC submodels represent tropospheric and stratospheric processes and their interaction with oceans, land and human influences, and describe emissions, radiative processes, atmospheric multiphase chemistry, aerosol and deposition mechanisms (Jöckel et al., 2006; Sander et al., 2005, 2011, 2014; Kerkweg et al., 2006; Tost et al., 2006, 2007; Pozzer et al., 2007, 2011; Pringle et al., 2010). We applied the EMAC model at T42/L31 spatial resolution, i.e., at a spherical spectral truncation of T42 and a quadratic Gaussian grid spacing of about 2.8 degrees latitude and longitude, and 31 hybrid terrain following – pressure levels up to 10 hPa.

Results have been evaluated against observations (Pozzer et al., 2010, 2012; de Meij et al., 2012; Christoudias and Lelieveld, 2013; Elshorbany et al., 2014; for additional references, see http://www.messy-interface.org). Here we present results based on emission fluxes and meteorology representative of the year 2013, mostly annual means unless specifically mentioned otherwise. Tests of the present model version indicate minor changes, e.g., in intermediately long-lived compounds such as O_3 and CO, compared to previous versions. N_2O and CH_4 concentrations have been prescribed at the surface based on observations. Natural emissions of higher VOCs are interactively calculated, amounting to 747–789 TgC/yr (including about 73%, or 546–578 TgC/yr, of isoprene) (Guenther et al., 2012), and anthropogenic emissions of saturated, unsaturated and aromatic compounds amount to 105 TgC/yr. These flux integrals are in carbon equivalent. It should be mentioned that in previous generation atmospheric chemistry-transport models VOC emissions have been artificially reduced to prevent the collapse of OH concentrations in regions of strong natural sources, i.e., at high-VOC and low-NO_X conditions (Arneth et al., 2010).

To analyze model production and sink pathways of OH and HO_2, including multiple radical recycling, and compute fluxes of reactants and intermediate products, we used the kinetic chemistry tagging technique of Gromov et al. (2010). The

Atmos. Chem. Phys. Discuss., doi:10.5194/acp-2016-160, 2016
Manuscript under review for journal Atmos. Chem. Phys.
Published: 11 March 2016

Atmospheric Chemistry and Physics Discussions

scheme computes detailed turnover rates of selected tracers, in this case OH, HO_2, O_3, CO, aldehydes, peroxides and others, in various parts of the MOM chemistry scheme within EMAC. With limited additional computational load the extensive budgeting allows characterization of OH sources and sinks, while the diagnostic calculations are decoupled from the regular chemistry scheme.

Here we present a selection of results, focusing on annual and large-scale averages to characterize global OH. The Supplement presents supporting tables and figures for the interested reader. Pages S1-S14 illustrate time sequences (Hovmöller plots), seasonal differences and results for different atmospheric environments and reservoirs such as the boundary layer (BL) and free troposphere (FT), to distinguish continental from marine boundary layers (CBL and MBL), the lower troposphere from the tropopause region and the lower stratosphere. These supplementary results focus on distributions of OH and HO_2, and lifetimes of different species, notably OH, HO_2, CO and CH_4, and include figures of global OH reactivity which may be relevant for the discussion in Sect. 5. Page S15 presents details on the global OH budget, relevant for Sect. 6. The Supplement also includes scatter plots between observations and model results of CO and O_3 at the surface for the year 2013 (S16), a table with details of VOC emission fluxes applied in EMAC (S17), and the complete mechanism of MOM, including a list of all chemical species (S18 and following). Model calculated global datasets of OH concentrations and other trace gases are available upon request.

3 Global OH distribution

In agreement with previous studies our model calculations show highest OH concentrations in the tropical troposphere (Fig. 1). Globally, mean tropospheric OH is $11.3 \cdot 10^5$ molecules/cm^3, close to the multi-model mean of $11.1 \pm 1.6 \cdot 10^5$ molecules/cm^3 derived by Naik et al. (2013) for the year 2000. Note that these are volume weighted means. Following the recommendation by Lawrence et al. (2001) we also calculated the air mass weighted ($11.1 \cdot 10^5$ molecules/cm^3), CH_4 weighted ($12.4 \cdot 10^5$ molecules/cm^3) and methyl chloroform (MCF) weighted means ($12.3 \cdot 10^5$ molecules/cm^3), though henceforth primarily report volume weighted mean values.

The calculated tropical tropospheric average is $14.6 \cdot 10^5$ molecules/cm^3 (between Tropics of Cancer and Capricorn), with the NH and SH extra-tropical averages being 9.1 and $6.6 \cdot 10^5$ molecules/cm^3, respectively. Our model indicates more OH north of the Equator compared to the south, 12.1 and $10.1 \cdot 10^5$ molecules/cm^3, respectively. Hence the NH/SH ratio is 1.20, being towards the low end of the multi-model estimate of 1.28 ± 0.10 by Naik et al. (2013), though deviating from inter-hemispheric parity derived by Patra et al. (2014) based on the analysis of MCF (CH_3CCl_3) measurements.

For the air mass, CH_4 and MCF weighted means we find NH/SH ratios of 1.25, 1.30 and 1.25, respectively. Part of the discrepancy with Patra et al. (2014) may be related to the seasonally varying position of the Inter-Tropical Convergence Zone (ITCZ), which effectively separates the meteorological NH from the SH. The position of the ITCZ, on average a few degrees north of the equator in the region of highest OH, can influence these calculations, both in models and MCF analyses. If we correct for this, the volume weighted NH/SH ratio of OH decreases from 1.20 to 1.13. In the extra-tropics our model calculates 28% less OH in the SH compared to the NH, being the main reason for the model calculated inter-hemispheric OH disparity. The difference is even larger between the Arctic and Antarctic regions (defined by the polar circles), as the calculated mean OH concentration is 50% lower in the latter. However, if we also include the lower stratosphere (up to 10 hPa) we find near-interhemispheric parity of OH, i.e., 5% more in the NH and only 2% more based on the ITCZ metric. Considering the importance of the stratosphere as an MCF reservoir to the troposphere in recent years (Krol and Lelieveld, 2003), and possible inter-hemispheric differences in the age-of-air in the middle atmosphere, these aspects should be investigated further with a model version that accounts for the atmosphere from the surface to the mesopause, to investigate the importance for MCF analyses and inferred OH distributions.

Fig. 1 illustrates that high OH concentrations in the tropics can extend up to the tropopause, with a main OH maximum below 300-400 hPa and a second maximum between 200 and 150 hPa. These oxidative conditions throughout the tropical troposphere limit the flux of reduced and partly oxidized gases (e.g., reactive halocarbons, sulfur and nitrogen gases) into the stratosphere through their chemical conversion into products that are removed by deposition processes. Near the cold tropical tropopause reaction products, such as low-volatile acids, can be removed by adsorption to sedimenting ice particles that also dehydrate the air that ascends into the stratosphere (Lelieveld et al., 2007). Due to the slow ascent rates of air parcels in the tropical tropopause region (tropical transition layer), pollutant gases are extensively exposed to oxidation by OH for several weeks to months. This mechanism protects the ozone layer from O_3 depleting substances that could be transported from the troposphere, at least to the extent that they react with OH.

In the global troposphere annual column average OH ranges from 1.0 to $22.0 \cdot 10^5$ molecules/cm^3, i.e., between high and low latitudes, respectively (Fig. 1). This range is determined by the meridional OH gradient in the FT, since about 85% of tropospheric OH formation takes place in the FT, which dominates the global OH distribution (detailed below). In the BL the range is much larger, 0.3 to $44.0 \cdot 10^5$ molecules/cm^3, as OH is affected by variable surface emissions. The subordinate role of the BL in the global OH load and distribution is conspicuous, for example from the OH maximum in the BL over the Middle East and OH minima over the Central African and Amazon forests (Fig. S1 of Supplement), which do not appear in the tropospheric column average OH concentrations, as the latter follow the OH distribution in the FT (Fig. 1).

In the BL over tropical forests OH concentrations are comparatively low, about 5 to $20 \cdot 10^5$ molecules/cm^3, while in the FT in these regions OH concentrations are several times higher. High OH in the tropical FT is partly related to the combination of emissions from vegetation with NO_X from lightning in deep thunderstorm clouds. This is most prominent over Central Africa where deep convection and lightning are relatively intense (Fig. 1, left panel). The chemical mechanisms that control OH in the BL and FT are connected through vertical transport and mixing, which balances formation and loss in the column, i.e., near the surface VOCs are a net sink of OH while their reaction products are a net OH source aloft.

In the NH extra-tropics mean OH in the MBL approximately equals that in the CBL, i.e., in the zonal direction. As shown previously, this is related to the transport and mixing of oxidants (primarily O_3) and precursor gases (e.g., NO_X and partially oxidized volatile organic compounds, OVOCs) from polluted regions across the Atlantic and Pacific Oceans (Lelieveld et al., 2002). In the SH, on the other hand, where anthropogenic NO_X sources and related transport are much less

Atmos. Chem. Phys. Discuss., doi:10.5194/acp-2016-160, 2016
Manuscript under review for journal Atmos. Chem. Phys.
Published: 11 March 2016

important, mean OH in the CBL is about 15% higher compared to the MBL. In the extra-tropical troposphere as a whole, OH gradients in the longitudinal direction are typically small (Fig. 1), related to relatively rapid exchanges by zonal winds in transient synoptic weather systems.

While primary OH formation during daytime is controlled by photo-dissociation of O_3, there are additional sources that can be relevant at night. This includes reactions of O_3 with unsaturated hydrocarbons and aromatic compounds in polluted air and with terpenes emitted by vegetation. Fig. 2 shows nighttime OH in the boundary layer during January and July to illustrate the strong seasonal dependency. While the color coding is the same as Fig. 1, the concentrations are scaled by a factor 20. On a global scale, OH concentrations in the BL at night are nearly two orders of magnitude lower than during the day, and in the FT diel differences are even larger. Therefore, nighttime OH does not significantly influence the atmospheric oxidation capacity and the lifetime of CH_4 and CO. Nevertheless, Fig. 2 shows several hotspots, mostly in the subtropical BL in the NH during summer, where nighttime OH can exceed 10^5 molecules/cm^3 and could contribute to chemical processes such as new particle formation. These regions include the Western USA, the Mediterranean and Middle East, the Indo-Gangetic Plane and Eastern China.

4 Global HO_X distribution

Fig. 3 shows the annual HO_2 concentration distribution, the counterpart of OH in Fig. 1. We find that in the BL annual mean HO_2 ranges from 0.1 to $6.4\cdot10^8$ molecules/cm^3 globally, whereas in the FT as a whole this is only 0.2 to $1.1\cdot10^8$ molecules/cm^3. Even though the mean lifetime of HO_2 in the troposphere of 1.5 minutes is much longer than of OH (factor 60), both OH and HO_2 are locally controlled by chemistry. Therefore, we refer to OH+HO_2 as HO_X. Transport processes influence HO_X through longer-lived precursor and reservoir species such as O_3 and OVOCs. Whereas OH in the BL over the tropical forests is relatively low, HO_2 is relatively high, about $5\cdot10^8$ molecules/cm^3, i.e., 2 to 3 orders of magnitude higher than OH, consistent with observations (Kubistin et al., 2010). Our results suggest that HO_X is highest over the tropical forests globally, where photochemistry is very active and OH sources and sinks are large. Localized HO_X maxima are also found in the polluted CBL where reactive VOC and NO_X emissions are strong, e.g., by the petroleum industry north of the Mexican Gulf and near the Persian Gulf.

On a global scale the tropospheric production of HO_2 – and thus HO_X – is dominated by that in the FT. In the FT HO_X is subject to long-range transport of relatively long-lived source and sink gases such as O_3 and CO, whereby the latter redistributes OH into HO_2 within HO_X, whereas in the BL local emissions of short-lived VOCs and NO_X are more relevant. The efficient atmospheric transport of longer-lived gases, such as O_3 from the stratosphere and O_3 from photochemically polluted regions, helps buffer the OH formation in regions where oxidant is depleted, such as the MBL. Within the tropospheric column, convection and entrainment of O_3 rich air from the FT into the BL play a key role in the exchange of oxidant, which reduces vertical gradients, and balances HO_X production and loss processes across altitudes.

Atmos. Chem. Phys. Discuss., doi:10.5194/acp-2016-160, 2016
Manuscript under review for journal Atmos. Chem. Phys.
Published: 11 March 2016

We calculate a global tropospheric average HO_2 concentration of $0.6 \cdot 10^8$ molecules/cm^3. We find the same average concentrations in the tropical and NH extra-tropical troposphere, and slightly less in the SH extra-tropics ($0.5 \cdot 10^8$ molecules/cm^3). Thus the mean tropospheric HO_2 (and HO_X) concentrations in these tropical and extra-tropical reservoirs are very similar. In the SH the mean HO_2 concentration in the CBL is about a factor 2 higher compared to the MBL, associated with strong VOC emissions by vegetation subject to intense photochemistry. In the NH mean HO_2 is comparable in the MBL and CBL, due to the widespread impact of air pollution, as explained above. The seasonal differences in tropospheric HO_X at middle and high latitudes can be large, i.e., about an order of magnitude between summer and winter. Nevertheless, the seasonality of primary OH formation, *P*, which is proportional to solar radiation intensity, is even larger. In Sec. 6 we discuss that the low *P* in winter is partly compensated by secondary OH formation.

5 Trace gas lifetimes and OH reactivity

The average tropospheric lifetime of OH (τ_{OH}) is 1.5s, calculated by relating the annual averages of the volume-weighted OH burden and the total photochemical sink rate. Fig. 4 presents the spatial distribution of τ_{OH}. In contrast to the OH concentration, τ_{OH} does not exhibit a strong seasonal cycle, being nearly absent in the tropics and the FT. Only in the CBL over Siberia, around 60°N, seasonal differences can reach a factor 5, related to the annual variability of VOC emissions by boreal forest (Siberian taiga). The tropospheric mean τ_{OH} in the NH is 1.4s and in the SH 1.6s. In the MBL mean τ_{OH} is about 0.7s, in the CBL about 0.3s. The seasonality of τ_{HO2} is more pronounced than of τ_{OH}; τ_{HO2} is longest in the cold season and over Antarctica, up to 10 minutes. In the MBL τ_{HO2} is on average 1.3 minutes, in the CBL 0.5 and in the FT 1.7 minutes.

We find that τ_{OH} is generally shortest over the tropical forest, followed by the boreal forest, coincident with the spatial distribution of total OH reactivity, i.e., the inverse of τ_{OH}, shown in Fig. 5. Near the Earth's surface the OH reactivity varies from about 0.5 s^{-1} over Antarctica, due to reaction of OH with CH_4 and CO in clean and cold air, to more than 100 s^{-1} over the Amazon rainforest in the dry season due to relatively strong isoprene sources, complemented by biomass burning emissions. This modeled OH reactivity range seems realistic in comparison to observations, whereas previous models – as well as measurement techniques – that did not account for all VOC reaction intermediates, strongly underestimated OH reactivity (Nölscher et al., 2016). This topic will be studied in greater detail in a follow-up publication where we address the reactive carbon budget in different environments, evaluated against measurements, including secondary organic aerosols (Tsimpidi et al., 2016).

The longest τ_{OH} is found near the tropical tropopause (10-20s) where OH reactivity is thus below 0.1 s^{-1}. While this is partly related to low temperatures and reduced reaction rates, it also indicates that air masses that traverse the tropical transition layer (TTL) into the stratosphere have been largely cleansed from compounds that react with OH. In the NH mean tropospheric OH reactivity is 0.7 s^{-1}, and in the SH 0.6 s^{-1}. On a side note, sulfur dioxide (SO_2) can largely pass the TTL because its reaction with OH is slow. Perhaps this serves a purpose in the Earth system because alternatively strong tropical

Atmos. Chem. Phys. Discuss., doi:10.5194/acp-2016-160, 2016
Manuscript under review for journal Atmos. Chem. Phys.
Published: 11 March 2016

volcano eruptions that inject large amounts of SO_2 could deplete OH below the tropopause so that other gases, including O_3 destroying halocarbons, could pass through and pose a threat to the stratospheric ozone layer.

Our estimate of the tropospheric mean lifetime of CH_4 due to oxidation by OH (τ_{CH4}) is 8.5 years, being within the multi-model calculated mean and standard deviation of 9.7±1.5 years presented by Naik et al. (2013), though towards the lower end of the range. Notice that this figure does not include uptake of CH_4 by soils and stratospheric loss by OH, $O(^1D)$ and chlorine radicals, which together make up about 10% of the total CH_4 sink. At the tropopause and the poles τ_{CH4} is longest, about a century. The effective difference in oxidation capacity of the high compared to the low-latitude troposphere is a factor ten, which is close to the extra-tropical seasonal cycle of HO_X. This is smaller than the low-to-high latitude gradients and the seasonal cycle of primary OH formation, indicative of the important role of secondary formation (Sec. 6). The NH/SH ratio of τ_{CH4} is 0.77. Similar differences and latitude contrasts are found for the lifetime of tropospheric CO (τ_{CO}) due to reaction with OH. In the tropics τ_{CO} is on average about 38 days, in the NH extra-tropics 65 days, in the SH extra-tropics 86 days, and the NH/SH ratio of τ_{CO} is 0.87.

6 Radical budgets and recycling probability

Table 1 and Fig. 6 present an overview of global, annual mean HO_X production terms in the troposphere. Primary OH formation (*P*, purple), amounts to 84 Tmol/yr, of which about 85% takes place in the FT. We find that gross OH formation (*G*) and HO_2 production in the FT also account for about 85% of the tropospheric total. Secondary OH formation (*S*) in the troposphere adds up to 167 Tmol/yr, i.e., 67% of *G*, the latter being 251 Tmol/yr. Fig. 6 illustrates that the fractional contributions by the different production terms in the FT equal those in the troposphere as a whole. It is not surprising that the FT is the dominant reservoir in atmospheric oxidation as it contains 6-7 times more mass than the BL, though it shows that OH formation is rather evenly distributed between different environments within the troposphere, in spite of differences in precursors species and pollution levels.

On a global scale, the relative magnitudes of different OH production terms in the BL and FT are similar (Fig. 6), though the OVOC mechanism (red) is somewhat larger, and the O_X mechanism through R11 (O_3+HO_2, green) plus R12 (H_2O_2+hv, yellow) is somewhat smaller than in the FT. The contribution by the NO_X mechanism, i.e., R7 (NO+HO_2, blue), is slightly smaller in the BL (30%) than the FT (31%), in spite that large areas in the BL are more directly influenced by anthropogenic NO_X emissions. As explained above, the catalytic role of NO_X in OH recycling is self-limiting, e.g., in the polluted BL, while some NO_X – partly as reservoir gases like organic nitrates – can escape to the FT where relatively lower concentrations can be effective in OH production. Examples of NO_X reservoir gases in MOM are alkyl nitrates with carbonyls, e.g., nitrooxyacetone (NOA) and the nitrate of methyl ethyl ketone.

By comparing *G* between different regions we find that it is about twice as high in the tropics than the extra-tropics, and 16% lower in the SH than the NH. On average, over the oceans *G* is the same as over the continents. Since emissions that affect OH largely occur on land, the latter underscores that on a large scale OH is buffered through processes in the FT.

Atmos. Chem. Phys. Discuss., doi:10.5194/acp-2016-160, 2016
Manuscript under review for journal Atmos. Chem. Phys.
Published: 11 March 2016

Regional maxima of *G* are found over the Amazon, Central Africa and southeastern Asia, and smaller areas north of the Mexican Gulf in the USA, Central America and Indonesia (Fig. 7). Over the Amazon and Central Africa we find a relatively high *G* up to the tropopause, related to deep convection and lightning over regions that are rich in natural VOCs. Within the BL *G* can vary greatly, e.g., being on average more than 3 times larger in the CBL than in the MBL. Comparing *P* between different regions we find that it is 37% higher in the tropics compared to the subtropics, while on average it is the same over oceans and continents.

Consequently, *S* is also the same over oceans and continents, though below we underscore that the underlying chemical mechanisms can be very different. In the SH extra-tropics *P* is about 40% lower than in the NH, mostly associated with the lower abundance of tropospheric O_3 in the SH. This inter-hemispheric asymmetry is manifest in the middle panels of Fig. 7. Comparison of the middle and lower panels in Fig. 7 shows that spatial gradients of *P* and *S* can be rather different, especially towards high latitudes and high altitudes where *P* declines steeply with solar radiation and water vapor. In these regions gradients of *S* are weaker than of *P*. This actually contributes to OH buffering, because the relatively low rate of *P* is partly compensated by *S*. This mechanism also acts seasonally, i.e., *S* is relatively more important in winter.

Rohrer et al. (2006, 2014) emphasized the tight linear relationship between tropospheric OH and UV radiation in Germany and China, expressed by measurements of OH and the photo-dissociation frequency of O_3 ($J(O^1D)$). While the relationship with sunlight is also evident from our results, the interpretation is not straightforward because *P* also depends on O_3 and H_2O, and *S* on many other factors. For example, in the tropics *P* has a maximum in the lower troposphere and a minimum in the upper troposphere at similarly high UV intensity, related to dependencies of the $J(O^1D)$ quantum yield and H_2O on temperature. Hence the slope of the regression is different. Furthermore, *S* is not contingent on $J(O^1D)$ and is generally less strongly dependent on solar radiation.

This is illustrated by Fig. 8, indicating that sometimes a tight linear relationship with $J(O^1D)$ is found, e.g., for *P* in the BL, but that the relationship with *S* in the BL is less compact, while in the FT *S* can deviate from linearity at low UV intensity. Based on a global sample size of 1.45 million pairs from our model calculations, we find a high correlation R^2=0.94 between *P* and $J(O^1D)$, and a lower correlation R^2=0.80 between *S* and $J(O^1D)$. While the mean slope for *P* is 0.99 (intercept close to zero), it is 0.46 for *S* (intercept about 0.3). Therefore, there is no unique relationship between OH and UV radiation as it depends on the relative importance of *P*, *S* and the different mechanisms that contribute to *S*.

Fig. 9 presents two illustrations of the efficiency at which OH is recycled. We find relatively large differences between tropospheric reservoirs, e.g., between the CBL and MBL, and also between the tropics and extra-tropics. The left panels show the relative contributions of primary and secondary OH formation to the total turnover of OH, $(S–P)/G$, which can be seen as the recycling efficiency. The right panels show the recycling probability $r=1–P/G$. When *S* is subordinate to *P*, the recycling efficiency is negative (orange and brown), which is the case in the clean MBL in the tropics and the mid-latitudes in the SH. In these environments *r* is below 50% (yellow and brown). However, if we consider the troposphere as a whole, *S* exceeds *P* everywhere due to the predominance of OH recycling in the FT. In the low latitude MBL *r* is lowest, indicative of a relatively high sensitivity to perturbations such as large-scale variations and trends in CH_4 and CO. This is not the case in the continental troposphere where natural VOCs play an important role in OH recycling. Fig. 9 shows that *r* is larger in the extra-tropics than in the tropics, and largest at high latitudes. In the BL the recycling eficiency and *r* anti-correlate with latitude and therefore with solar radiation intensity.

The chemical buffering mechanisms include the dominant though self-limiting effect of NO_X on OH formation in polluted air, the latter through reaction R10, which is an important sink of both NO_2 and OH when concentrations are high (NO_X mechanism). In unpolluted, low-NO_X conditions the OVOC mechanism acts through competition of unsaturated peroxide and carbonyl sinks, e.g., hydroperoxide-aldehyde (HPALD) in isoprene chemistry. When OH is high, HPALD reacts with OH, whereas at low OH photo-dissociation takes the upper hand through the formation of peroxy-acid aldehyde (PACALD), which produces OH. Over land OH is generally buffered by the NO_X and OVOC mechanisms, illustrated by values of *r* well over 50% (Fig. 9). However, remote from NO_X and VOC sources in the BL over the tropical and subtropical oceans *r* can be below 40%. In these environments OH recycling depends on the O_X mechanism, which has limited efficiency because R11 (O_3+HO_2) is a net oxidant sink. Hence the O_X mechanism depends on replenishment of O_3 through transport in the FT.

Differences in *S* between tropospheric reservoirs, e.g., the CBL, MBL, tropics and extra-tropics, are associated with these three principal OH recycling mechanisms, to various degrees related to natural and anthropogenic VOC and NO_X emissions. Fig. 10 illustrates how OH is buffered both on local and global scales. It shows the fractional contributions of the NO_X, O_X and OVOC mechanisms to the overall recycling probability *r*. The complementarity of the three mechanisms is remarkable. The NO_X mechanism dominates in the NH, especially in polluted air at middle latitudes, and most strongly over the continents. In the SH over the continents, in low-NO_X air, the OVOC mechanism dominates. In the marine environment – except the pollution outflow regions over the Atlantic and Pacific Oceans – the O_X mechanism predominates. Seasonal complementarity of the three mechanisms is most significant at high latitudes, especially in the BL. Whereas in summer the O_X mechanism is most efficient, and to a lesser degree also the NO_X mechanism, in winter the OVOC mechanism maintains OH formation, being least dependent on solar radiation.

7 Conclusions

The atmospheric oxidation capacity is generally buffered against perturbations that may arise from variations or trends in emissions of natural and anthropogenic origin. This is illustrated by global OH calculations with a large number of chemistry-transport models (Naik et al., 2013; Voulgarakis et al., 2013), where differences between models are larger than between pre-industrial, present and future emission scenarios calculated by the same models. This suggests that model physics and chemistry formulations have a greater impact on calculations of global OH than applying different emission scenarios of source and sink gases. Results from the EMAC atmospheric chemistry – general circulation model illustrate how a combination of tropospheric chemistry and transport mechanisms buffer OH on a range of scales.

Atmos. Chem. Phys. Discuss., doi:10.5194/acp-2016-160, 2016
Manuscript under review for journal Atmos. Chem. Phys.
Published: 11 March 2016

The EMAC model includes the recent Mainz Organics Mechanism (MOM) to comprehensively account for VOC chemistry, including higher generation reaction products, leading to a closed atmospheric budget of reactive carbon. The more realistic description of emissions and complex VOC chemistry in MOM compared to previous models substantially increases OH reactivity. We also find that in the polluted CBL, notably in the subtropical NH during summer, nighttime VOC chemistry initiated by O_3 can produce OH concentrations in excess of 10^5 molecules/cm^3, which may be relevant for particle nucleation, for example. Nevertheless, nighttime OH does not contribute significantly to the atmospheric oxidation capacity (e.g., τ_{CH4} and τ_{CO}).

Global mean OH concentrations in the BL equal those in the FT and thus the troposphere as a whole ($11.3 \cdot 10^5$ molecules/cm^3). Tropospheric column averaged OH concentrations are highest in the tropics, especially over the Amazon, Central Africa and Southeast Asia. Concentrations of HO_X ($OH+HO_2$) are highest in the CBL over the Amazon, Central Africa, Southeast Asia, and relatively smaller regions over North Australia, the USA north of the Mexican Gulf and near the Persian Gulf. The latter is related to emissions from the petroleum industry in photochemically polluted air.

While measurement campaigns often focus on the BL, the global distribution and variability of OH and HO_X are dominated by the FT. Long-distance transport processes and OH recycling are most efficient in the FT, whereas BL chemistry is typically sensitive to local impacts of reactive carbon emissions. Physical-chemical tele-connections in the FT play an important role in global OH buffering through oxidant transport, notably of ozone. The FT connects with the BL through convective mixing by clouds (latent heating) and entrainment by the diurnal evolution of the BL (sensible heating). The latter is more effective in the continental than in the marine environment.

While HO_X concentrations can diverge strongly over the globe, especially in the BL and between seasons, annual averages in the troposphere vary little, e.g., between the tropics and extra-tropics and between hemispheres. Tropospheric OH is buffered through complementary primary and secondary formation mechanisms throughout seasons, latitudes and altitudes. We find that primary OH formation is tightly coupled to solar UV radiation intensity, whereas this is much less the case for secondary OH formation. There are three principal pathways of secondary OH formation: the NO_X, O_X and OVOC mechanisms.

The NO_X mechanism predominates in anthropogenically influenced environments, causing photochemical smog, and outcompetes the OVOC mechanism concomitant with VOC emissions from vegetation. On the other hand, when NO_X is low the photochemistry of natural VOCs, through OVOC reaction products, governs radical recycling and maintains the atmospheric oxidation capacity associated with undisturbed atmosphere-biosphere interactions. When both NO_X and VOC concentrations are low, e.g., in the remote marine environment and at high latitudes, OH recycling strongly depends on the O_X mechanism.

Recycling mechanisms of OH are important near emission sources of NO_X and VOCs in regions of active photochemistry in the BL, but especially in remote areas and the FT when photochemistry is less active. On large scales ozone is a key buffer of OH. To a lesser degree NO_X reservoir species (nitrates) also play a role. On smaller scales H_2O_2 and OVOCs that release OH upon further reaction and photo-dissociation (e.g., organic peroxides and carbonyls) are important.

These short-lived reservoir species govern OH sources and sinks within the column. Ozone, with a lifetime of several weeks in the FT, maintains the atmospheric oxidation capacity through long-distance transport, either from the stratosphere or from photochemically polluted regions, in natural and anthropogenically influenced atmospheres, respectively.

References

Arneth, A, Harrison. S.P., Zaehle, S., Tsigaridis, K., Menon, S., Bartlein, P.J., Feichter, J., Korhola, A., Kulmala, M., O'Donnell, D., Schurgers, G., Sorvari, S., and Vesala, T.: Terrestrial biogeochemical feedbacks in the climate system, Nature Geosci., 3, 525-532, 2010.

Butler, T.M., Lawrence, M.G., Taraborrelli, D., and Lelieveld, J.: Tagged ozone production potential (TOPP) of volatile organic compounds, Atmos. Environ., 45, 4082-4090, 2011.

Christoudias, T., and Lelieveld, J.: Modelling the global atmospheric transport and deposition of radionuclides from the Fukushima Dai-ichi nuclear accident, Atmos. Chem. Phys., 13, 1425-1438, 2013.

Crounse, J.D., Knap, H.C., Ørnsø, K.B., Jørgensen, S., Paulot, F., Kjaergaard, G.G., and Wennberg, P.O.: Atmospheric fate of methacrolein. 1. Peroxy radical isomerization following addition of OH and O_2, J. Phys. Chem., A, 116, 5756-5762, 2012.

Crounse, J.D., Nielsen, L.B., Jørgensen, S., Kjaergaard, H.G., and Wennberg, P.O.: Autoxidation of organic compounds in the atmosphere, J. Phys. Chem. Lett., 4, 3513-3520, 2013.

Crutzen, P.J.: The role of NO and NO_2 in the chemistry of the troposphere and the stratosphere, Annu. Rev. Earth. Planet. Sci., 7, 443-472, 1979.

Crutzen, P.J., and Zimmermann, P.H.: The changing photochemistry of the troposphere, Tellus, 43AB, 136-151, 1991.

De Meij, A., Pozzer, A., Pringle, K.J., Tost, H., and Lelieveld, J.: EMAC model evaluation and analysis of atmospheric aerosol properties and distribution, Atmos. Res., 114-115, 38-69, 2012.

Ehhalt, D.H., Dorn, H.-P., and Poppe, D.: The chemistry of the hydroxyl radical in the troposphere, Proc. Roy. Soc. Edinburgh, Ser. B., 97, 17-34, 1991.

Elshorbany, Y.F., Crutzen, P., Steil, B., Pozzer, A., and Lelieveld, J.: Global and regional impacts of HONO on the chemical composition of clouds and aerosols, Atmos. Chem. Phys., 14, 1167-1184, 2014.

Fuchs, H., Acir, I.-H., Bohn, B., Brauers, T., Dorn, H.-P., Häseler, R., Hofzumahaus, A., Holland, F., Kaminski M., Li, X., Lu, K., Lutz, A., Nehr, S., Rohrer, F., Tillmann, R., Wegener, R., and Wahner, A., OH regeneration from methacrolein oxidation investigated in the atmosphere simulation chamber SAPHIR, Atmos. Chem. Phys., 14, 7895-7908, 2014.

Groß, C.B.M., Dillon, T.J., Schuster, G., Lelieveld, J., and Crowley, J.N., Direct kinetic study of OH and O_3 formation in the reaction of $CH_3C(O)O_2$ with HO_2, J. Phys. Chem., A, 118, 974-985, 2014a.

Groß, C.B.M., Dillon, T.J., and Crowley, J.N., Pressure dependent OH yields in the reactions of CH_3CO and $HOCH_2CO$ with O_2, Phys. Chem. Chem. Phys., 16, 10990-10998, 2014b.

Gromov, S., Jöckel, P., Sander, R., and Brenninkmeijer, C.A.M.: A kinetic chemistry tagging technique and its application to modelling the stable isotopic composition of atmospheric trace gases, Geosci. Model Dev., 3, 337-364, 2010.

Guenther, A.B., Jiang, X., Heald, C.L., Sakulyanontvittaya, T., Duhl, T., Emmons, L.K., and Wang, X.: The Model of Emissions of Gases and Aerosols from Nature version 2.1 (MEGAN2.1): an extended and updated framework for modeling biogenic emissions, Geosci. Model Dev., 5, 1471-1492, 2012.

Houweling, S., Dentener, F., and Lelieveld, J.: The impact of non-methane hydrocarbon compounds on tropospheric photochemistry, J. Geophys. Res., 103, 10673-10696, 1998.

Jenkin, M.E., Young, J.C., and Rickard, A.R.: The MCM v3.3.1 degradation scheme for isoprene, Atmos. Chem. Phys., 15, 11433-11459, 2015.

Jöckel, P., Sander, R., Kerkweg, A., Tost, H., and Lelieveld, J.: Technical Note: The Modular Earth Submodel System (MESSy) - a new approach towards Earth System Modeling, Atmos. Chem. Phys., 5, 433–444, 2005.

Jöckel, P., Tost, H., Pozzer, A., Brühl, C., Buchholz, J., Ganzeveld, L., Hoor, P., Kerkweg, A, Lawrence, M.G., Sander, R., Steil, B., Stiller, G., Tanarhte, M., Taraborrelli, D., van Aardenne, J., and Lelieveld, J.: The atmospheric chemistry general circulation model ECHAM5/MESSy: Consistent simulation of ozone from the surface to the mesosphere, Atmos. Chem. Phys., 6, 5067-5104, 2006.

Jöckel, P., Kerkweg, A., Pozzer, A., Sander, R., Tost, H., Riede, H., Baumgaertner, A., Gromov, S., and Kern, B.: Development cycle 2 of the Modular Earth Submodel System (MESSy2), Geoscientific Model Development, 3, 717–752, 2010.

Kerkweg, A., Sander, R., Tost, H., and P. Jöckel: Technical Note: Implementation of prescribed (OFFLEM), calculated (ONLEM), and pseudo-emissions (TNUDGE) of chemical species in the Modular Earth Submodel System (MESSy), Atmos. Chem. Phys., 6, 3603–3609, 2006.

Krol, M., and Lelieveld, J.: Can the variability in tropospheric OH be deduced from measurements of 1,1,1-trichloroethane (methyl chloroform)? J. Geophys. Res., 108, 4125, doi:10.1029/2002JD002423, 2003.

Kubistin, D., Harder, H., Martinez, M., Rudolf, M., Sander, R., Bozem, H., Eerdekens, G., Fischer, H., Gurk, C., Klüpfel, T., Königstedt, R., Parchatka, U., Schiller, C.L., Stickler, A., Taraborrelli, D., Williams, J., and Lelieveld, J.: Hydroxyl radicals in the tropical troposphere over the Suriname rainforest: comparison of measurements with the box model MECCA, Atmos. Chem. Phys., 10, 9705-9728, 2010.

Lawrence, M.G., Jöckel, P., and von Kuhlmann, R.: What does the global mean OH concentration tell us? Atmos. Chem. Phys., 1, 37-49, 2001.

Lelieveld, J., Peters, W., Dentener, F.J., and Krol: M. Stability of tropospheric hydroxyl chemistry, J. Geophys. Res., 107, 10.1029/2002JD002272, 2002.

Lelieveld, J., Brühl, C., Jöckel, P., Steil, B., Crutzen, P.J., Fischer, H., Giorgetta, M.A., Hoor, P., Lawrence, M.G., Sausen, R., and Tost, H.: Stratospheric dryness: model simulations and satellite observations, Atmos. Chem. Phys., 7, 1313-1332, 2007.

Lelieveld, J., Butler, T.M., Crowley, J.N., Dillon, T.J., Fischer, H., Ganzeveld, L., Harder, H., Lawrence, M.G., Martinez, M., Taraborrelli, D., and Williams, J.: Atmospheric oxidation capacity sustained by a forest, Nature, 452, 737-740, 2008.

Levy II, H.: Normal atmosphere: large radical and formaldehyde concentrations predicted, Science, 173, 141-143, 1971.

Logan, J.A., Prather, M.J., Wofsy, S.C., and McElroy, M.B.: Tropospheric chemistry: A global perspective, J. Geophys. Res., 86, 7210-7354, 1981.

Monks, P.S., Archibald, A.T., Colette, A., Cooper, O., Coyle, M., Derwent, R., Fowler, D., Granier, C., Law, K.S., Mills, G.E., Stevenson, D.S., Tarasova, O., Thouret, V., von Schneidemesser, E., Sommariva, R., Wild, O., and Williams, M.L.: Tropospheric ozone and its precursors from the urban to the global scale from air quality to short-lived climate forcer, Atmos. Chem. Phys., 15, 8889-8973, 2015.

Montzka, S., Krol, M., Dlugokencky, E., Hall, B., Jöckel, P., and Lelieveld, J.: Small inter-annual variability of global atmospheric hydroxyl, Science, 331, 67-69, 2011.

Naik, V., Voulgarakis, A., Fiore, A.M., Horowitz, L.W., Lamarque, J.-F., Lin, M., Prather, M.J., Young, J., Bergmann, D., Cameron-Smith, P.J., Cionni, I., Collins, W.J., Dalsøren, S.B., Doherty, R., Eyring, V., Faluvegi, G., Folberth, G.A., Josse, B., Lee, Y.H., MacKenzie, I.A., Nagashima, T., van Noije, T.P.C., Plummer, D.A., Righi, M., Rumbold, S.T., Skeie, R., Shindell, D.T, Stevenson, D.S., Strode, S., Sudo, K., Szopa, S., and Zeng, G.: Preindustrial to present-day changes in tropospheric hydroxyl radical and methane lifetime from the Atmospheric Chemistry and Climate Model Intercomparison Project (ACCMIP), Atmos. Chem. Phys., 13, 5277-5298, 2013.

Nölscher, A.C., Butler, T., Auld, J., Veres, P., Muñoz, A., Taraborrelli, D., Vereecken, L., Lelieveld, J., and Williams, J.: Using total OH reactivity to assess isoprene photooxidation via measurement and model, Atmos. Environ., 89, 453-463, 2014.

Nölscher, AC., Yanez-Serrano, A.M., Wolff, S., Carioca de Araujo, A., Lavric, J.V., Kesselmeier, J., and Williams, J.: Unexpected seasonality in quantity and composition of Amazon rainforest air reactivity, Nat. Commun., 7:10383, doi: 10.1038/ncomms10383, 2016.

Patra P.K., Krol, M.C., Montzka, S.A., Arnold, T., Atlas, E.L., Lintner, B.R., Stephens, B.B., Xiang, B., Elkins, J.W., Fraser, P.J., Ghosh, A., Hintsa, E.J., Hurst, D.F., Ishijima, K., Krummel, P.B., Miller, B.R., Miyazaki, K., Moore, F.L., Mühle, J., O'Doherty, S., Prinn, R.G., Steele, L.P., Takigawa, M., Wang, H.J., Weiss, R.F., Wofsy, S.C., and Young, D.: Observational evidence for interhemispheric hydroxyl-radical parity, Nature, 513, 219-223, 2014.

Paulot, F., Crounse, J.D., Kjaergaard, H.G., Kürten, A., St. Clair, J.M., Seinfeld, J.H., Wennberg, P.O., Unexpected epoxide formation in the gas-phase photooxidation of isoprene, Science, 325, 730-733, 2009.

Peeters, J., Müller, J.-F., Stavrakou, T., and Nguyen, V.S., Hydroxyl radical Recycling in isoprene oxidation driven by hydrogen bonding and hydrogen tunneling: The upgraded LIM1 mechanism, J. Phys. Chem., A, 118, 8625-8643, 2014.

Pozzer, A., Jöckel, P., Tost, H., Sander, R., Ganzeveld, L., Kerkweg, A., and Lelieveld, J.: Simulating organic species with the global atmospheric chemistry general circulation model ECHAM5/MESSy1: a comparison of model results with observations, Atmos. Chem. Phys., 7, 2527-2550, 2007.

Pozzer, A., Pollmann, J., Taraborrelli, D., Jöckel, P., Helmig, D., Tans, P., Hueber, J., and Lelieveld, J.: Observed and simulated global distribution and budget of atmospheric C2−C5 alkanes, Atmos. Chem. Phys., 10, 4403-4422, 2010.

Pozzer, A., Jöckel, P., Kern, B., and Haak, H.: The atmosphere-ocean general circulation model EMAC-MPIOM, Geosci. Model Dev., 4, 771-784, 2011.

Pozzer, A., de Meij, A., Pringle, K.J., Tost, H., Doering, U.M., van Aardenne, J., and Lelieveld, J.: Distributions and regional budgets of aerosols and their precursors simulated with the EMAC chemistry-climate model, Atmos. Chem. Phys., 12, 961-987, 2012.

Pringle, K.J., Tost, H., Metzger, S., Steil, B., Giannadaki, D., Nenes, A., Fountoukis, C., Stier, P., Vignati, E., and Lelieveld, J.: Description and evaluation of GMXe: A new aerosol submodel for global simulations (v1), Geosci. Model Develop., 3, 391-412, 2010.

Roeckner, E., Brokopf, R., Esch, M., Giorgetta, M., Hagemann, S., Kornblüh, Manzini, L. E., Schlese, U., and Schulzweida, U.: Sensitivity of simulated climate to horizontal and vertical resolution in the ECHAM5 atmosphere model, J. Climate, 19, 3771-3791, 2006.

Rohrer, F., and Berresheim, H.: Strong correlation between levels of tropospheric hydroxyl radicals and solar ultraviolet radiation, Nature, 442, 184-187, 2006.

Rohrer, F., Lu, K., Hofzumahaus, A., Bohn, B., Brauers, T., Chang, C.-C., Fuchs, H., Häseler, R., Holland, F., Hu, M., Kita, K., Kondo, Y., Li, X., Lou, S., Oebel, A., Shao, M., Zeng, L., Zhu, T., Zhang, Y., and Wahner, A.: Maximum efficiency in the hydroxyl-radical-based self-cleansing of the troposphere, Nature Geosc., 7, 559-563.

Sander, R., Kerkweg, A., Jöckel, P., and Lelieveld, J.: Technical Note: The new comprehensive atmospheric chemistry module MECCA, Atmos. Chem. Phys., 5, 445-450, 2005.

Sander, R. Baumgaertner, A., Gromov, S., Harder, H., Jöckel, P., Kerkweg, A., Kubistin, D., Regelin, E., Riede, H., Sandu, A., Taraborrelli, D., Tost, H., and Xie, Z.-Q.: The atmospheric chemistry box model CAABA/MECCA-3.0, Geosci. Model Dev., 4, 373-380, 2011.

Sander, R., Jöckel, P., Kirner, O., Kunert, A.T., Landgraf, J., and Pozzer, A.: The photolysis module JVAL-14, compatible with the MESSy standard, and the JVal PreProcessor (JVPP), Geosci. Model Dev., 7, 2653-2662, 2014.

Spivakovsky, C.M., Logan, J.A., Montzka, S.A., Balkanski, Y.J., Foreman-Fowler, M., Jones, D.B. A., Horowitz, L.A., Fusco, A.C., Brenninkmeijer, C.A.M., Prather, M.J., Wofsy, S.C., and McElroy, M.B.: Three-dimensional climatological distribution of tropospheric OH: Update and evaluation, J. Geophys. Res., 105, 8931-8980, 2000.

Stockwell, W.R., Lawson, C.V., Saunders, E., and Goliff, W.S.: A review of tropospheric atmospheric chemistry and gas-phase chemical mechanisms for air quality modeling, Atmosphere, 3, 1-32, 2012.

Stone, D., Whalley, L.K., and Heard, D.E.: Tropospheric OH and HO_2 radicals: field measurements and model comparisons, Chem. Soc. Rev., 41, 6348-6404, 2012.

Taraborrelli, D., Lawrence, M., Butler, T., Sander, R., and Lelieveld, J.: Mainz Isoprene Mechanism 2 (MIM2): an isoprene oxidation mechanism for regional and global atmospheric modeling, Atmos. Chem. Phys., 9, 2751-2777, 2009.

Taraborrelli, D., Lawrence, M.G., Crowley, J.N., Dillon, T.J., Gromov, S., Groß, C.B.M., Vereecken, L., and Lelieveld, J.: Hydroxyl radical buffered by isoprene oxidation over tropical forests. Nature Geosci. 5, 190-193, 2012.

Tost, H., Jöckel, P., Kerkweg, A., Sander, R., and Lelieveld, J.: Technical Note: A new comprehensive SCAVenging submodel for global atmospheric chemistry modelling, Atmos. Chem. Phys., 6, 565-574, 2006.

Tost, H., Jöckel, P., Kerkweg, A., Pozzer, A., Sander, R., and Lelieveld, J.: Global cloud and precipitation chemistry and wet deposition: tropospheric model simulations with ECHAM5/MESSy1, Atmos. Chem. Phys., 7, 2733-2757, 2007.

Tsimpidi, A.P., Karydis, V.A., Pandis, S.N., and Lelieveld, J.: Global combustion sources of organic aerosols: Model comparison with 84 AMS factor analysis data sets, Atmos. Chem. Phys. Discuss., doi:10.5194/acp-2015-989, 2016.

Vereecken, L., and Francisco, J.S., Theoretical studies of atmospheric reaction mechanisms in the troposphere, Chem. Soc. Rev., 41, 6259-6293, 2012.

Voulgarakis, A., Naik, V., Lamarque, J.-F., Shindell, D.T., Young, P.J., Prather, M.J., Wild, O., Field, R.D., Bergmann, D., Cameron-Smith, P., Cionni, I., Collins,W.J., Dalsøren, S.B., Doherty, R.M., Eyring, V., Faluvegi, G., Folberth, G.A., Horowitz, L.W., Josse, B., MacKenzie, I.A., Nagashima, T, Plummer, D.A., Righi, M., Rumbold, S.T., Stevenson, D.S., Strode, S.A., Sudo, K., Szopa, S., and Zeng, G.: Analysis of present day and future OH and methane lifetime in the ACCMIP simulations, Atmos. Chem. Phys., 13, 2563-2587, 2013.

Atmos. Chem. Phys. Discuss., doi:10.5194/acp-2016-160, 2016
Manuscript under review for journal Atmos. Chem. Phys.
Published: 11 March 2016

Table 1. Global, annual mean HO_X production terms (Tmol/yr); balanced by chemical loss and deposition (mainly H_2O_2).

	BL	FT	Troposphere
$O(^1D)+H_2O$	12.5	71.5	84.0
$NO+HO_2$	10.4	66.2	76.6
O_3+HO_2	3.5	30.9	34.5
$H_2O_2+h\nu$	2.3	22.5	24.8
OVOCs, ROOH+hν	6.5	24.8	31.4
Total OH source	35.3	215.9	251.2
Total HO_2 source	45.5	233.1	278.6
H_2O_2 deposition	3.8	–	3.8

Atmos. Chem. Phys. Discuss., doi:10.5194/acp-2016-160, 2016
Manuscript under review for journal Atmos. Chem. Phys.
Published: 11 March 2016

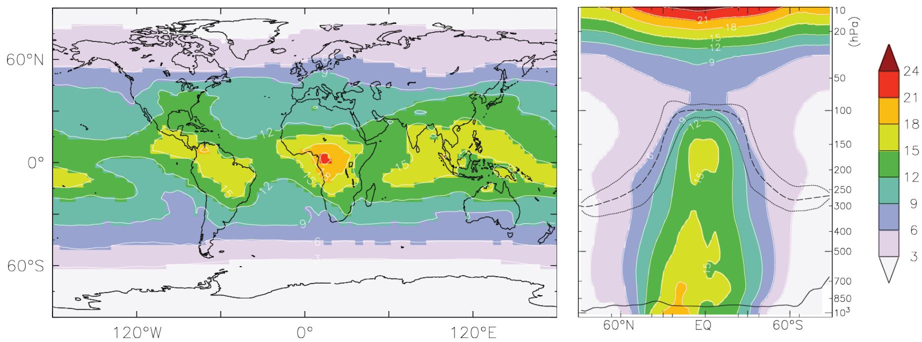

Figure 1: Global OH in 10^5 molecules/cm^3. Left: tropospheric, annual mean. Right: zonal, annual mean up to 10 hPa. The lower solid line indicates the average boundary layer height, the upper dashed line the mean tropopause and the solid lines the annual minimum and maximum tropopause height.

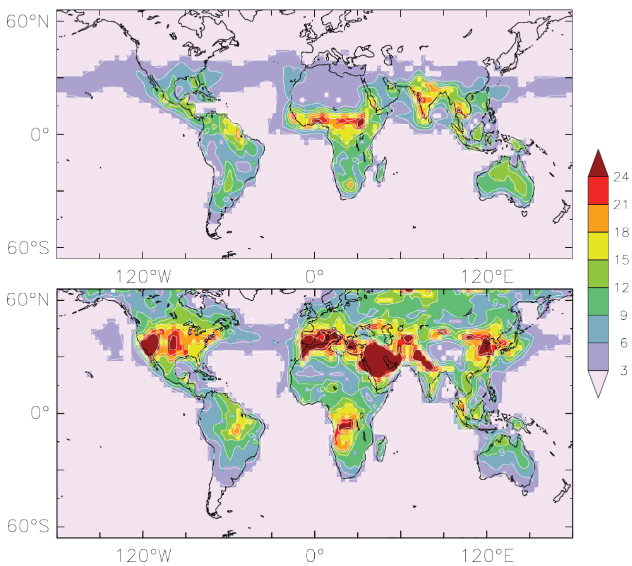

Figure 2: Nighttime OH in the boundary layer in January (top) and July (bottom). Color coding is the same as Fig. 1, but concentrations are scaled by a factor 20 (x0.05·10^5 molecules/cm^3).

Atmos. Chem. Phys. Discuss., doi:10.5194/acp-2016-160, 2016
Manuscript under review for journal Atmos. Chem. Phys.
Published: 11 March 2016

Atmospheric Chemistry and Physics
Open Access
Discussions

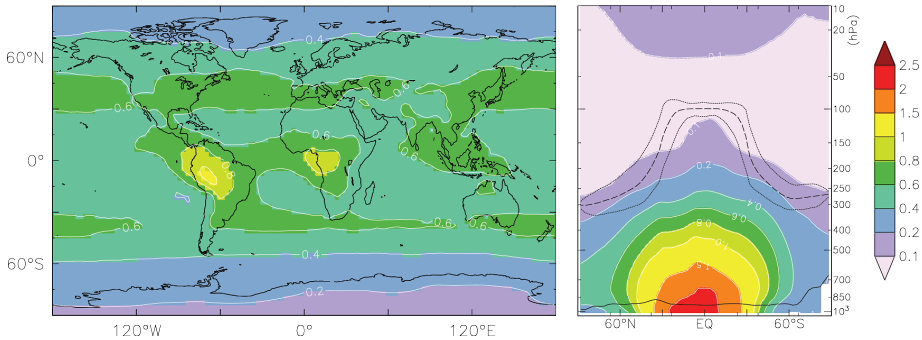

Figure 3: As Fig. 1 for HO_2 in 10^8 molecules/cm^3 in the troposphere (left) and up to 10 hPa (right).

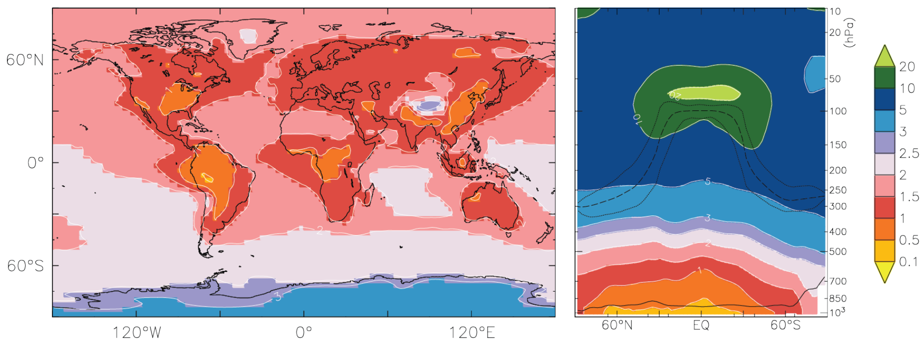

Figure 4: As Fig. 1 for the OH lifetime (τ_{OH}, seconds) in the troposphere (left) and up to 10 hPa (right).

Atmos. Chem. Phys. Discuss., doi:10.5194/acp-2016-160, 2016
Manuscript under review for journal Atmos. Chem. Phys.
Published: 11 March 2016

Atmospheric Chemistry and Physics
Discussions

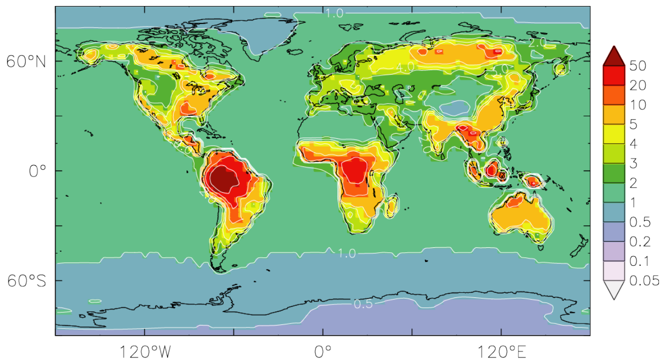

Figure 5: Annual mean OH reactivity near the Earth's surface in s^{-1}.

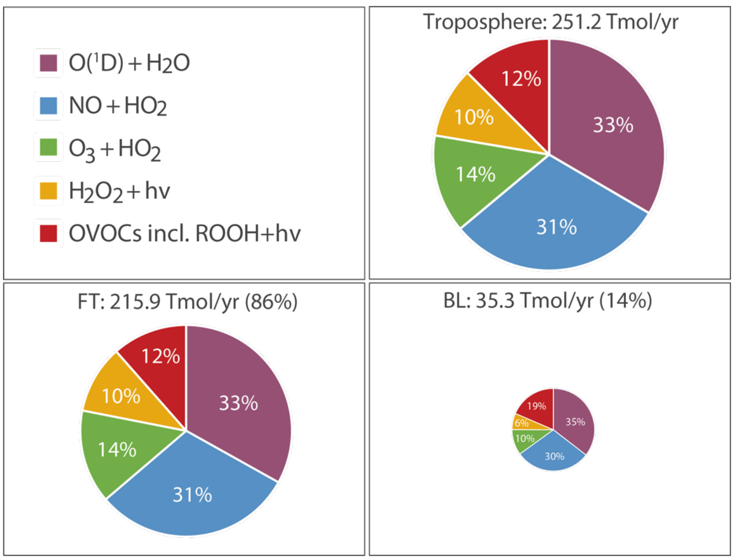

Figure 6: Main production terms of OH (Tmol/year) in the troposphere (top right), free troposphere (bottom left) and boundary layer (bottom right). The sizes of the lower two graphs are proportional to the upper right graph, reflecting the percentages of *G* in parentheses. We distinguish *P* (purple) from *S*, the latter made up of the NO_X mechanism (blue), the O_X mechanism (yellow and green) and the OVOC mechanism (red).

Atmos. Chem. Phys. Discuss., doi:10.5194/acp-2016-160, 2016
Manuscript under review for journal Atmos. Chem. Phys.
Published: 11 March 2016

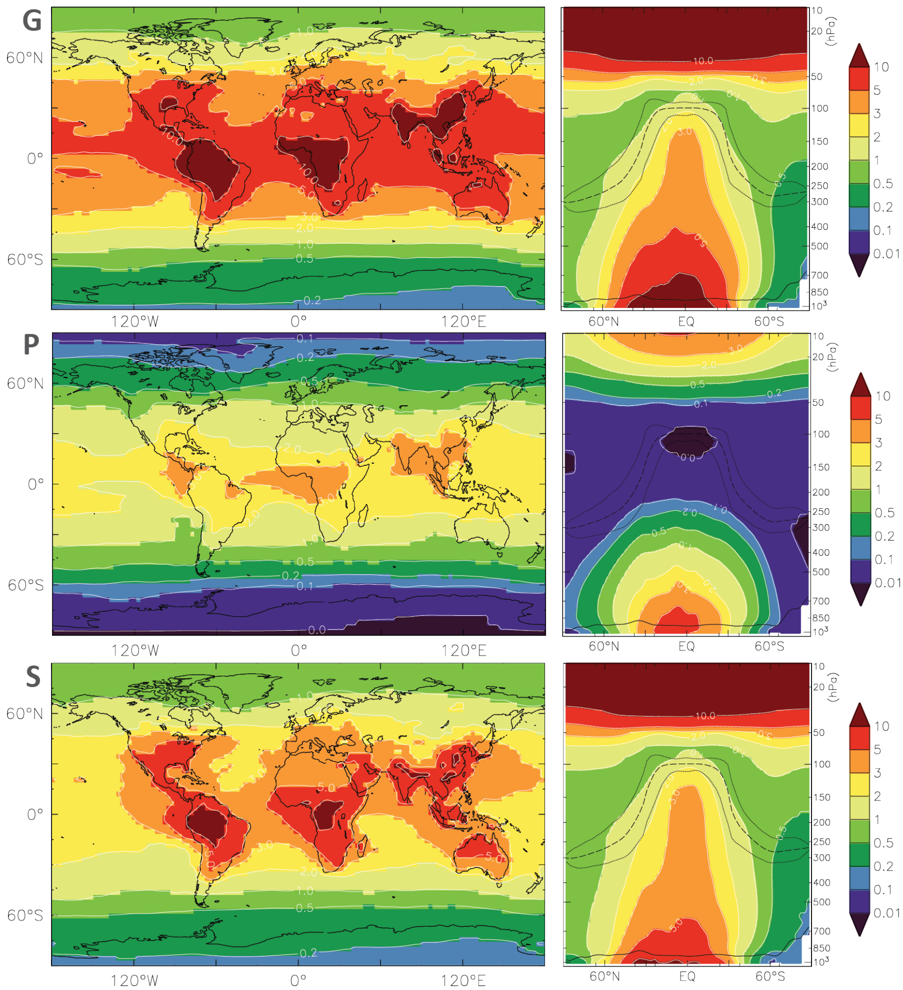

5

Figure 7: Annual mean OH formation in the troposphere (left) and up to 10 hPa (right). The top panels show total (*G*), the middle panels primary (*P*) and the bottom panels secondary (*S*) OH formation.

Atmos. Chem. Phys. Discuss., doi:10.5194/acp-2016-160, 2016
Manuscript under review for journal Atmos. Chem. Phys.
Published: 11 March 2016

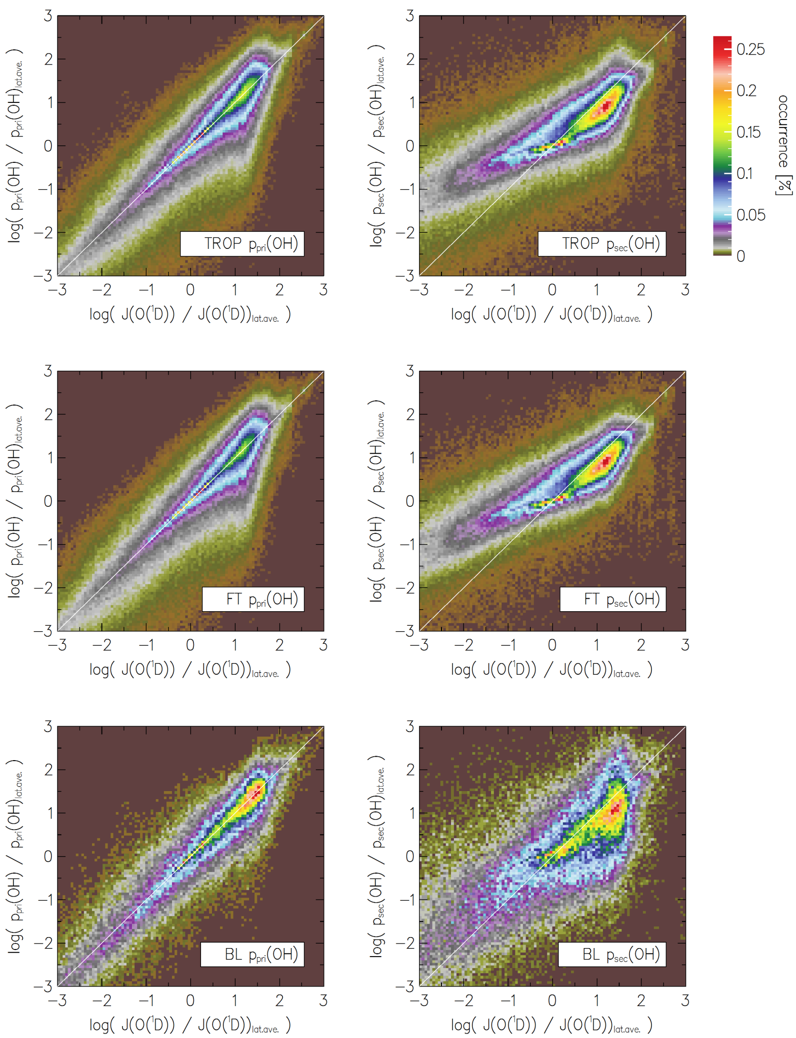

Figure 8: Correlation diagrams, showing *P* and *S* on the Y-axes as a function of the photo-dissociation rate of O_3 by R1, J(O^1D), on the X-axes. Please notice the log/log scale. *P* is shown in the left panels and *S* in the right panels, in the troposphere (top), FT (middle) and BL (bottom).

Atmos. Chem. Phys. Discuss., doi:10.5194/acp-2016-160, 2016
Manuscript under review for journal Atmos. Chem. Phys.
Published: 11 March 2016

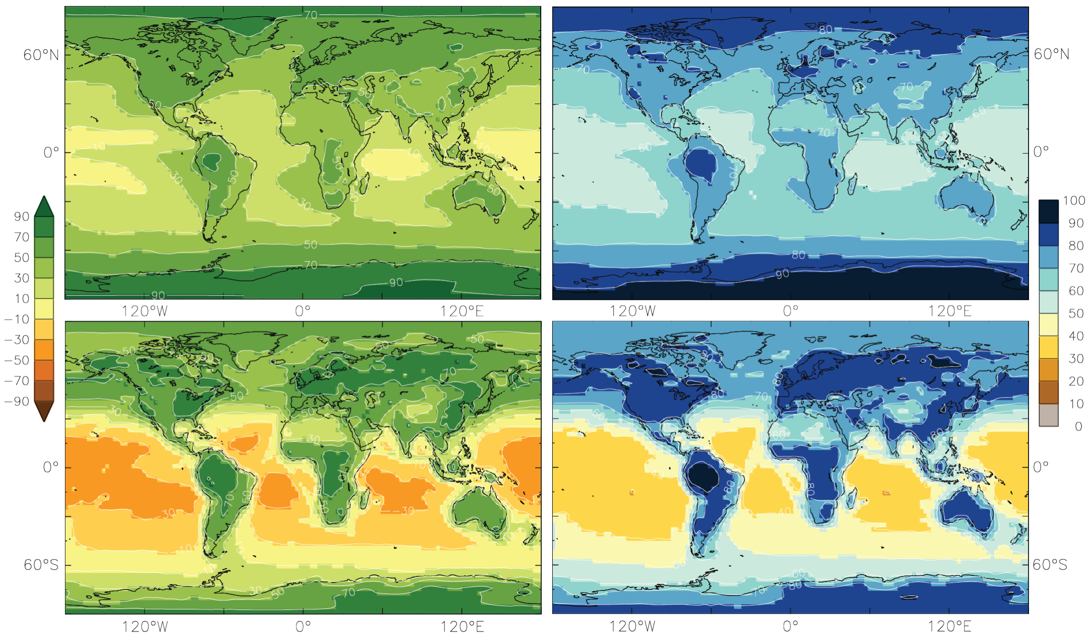

Figure 9: Annual mean OH recycling efficiency (left, in %), and the OH recycling probability (right, *r* in %) in the troposphere (top) and the BL (bottom).

Atmos. Chem. Phys. Discuss., doi:10.5194/acp-2016-160, 2016
Manuscript under review for journal Atmos. Chem. Phys.
Published: 11 March 2016

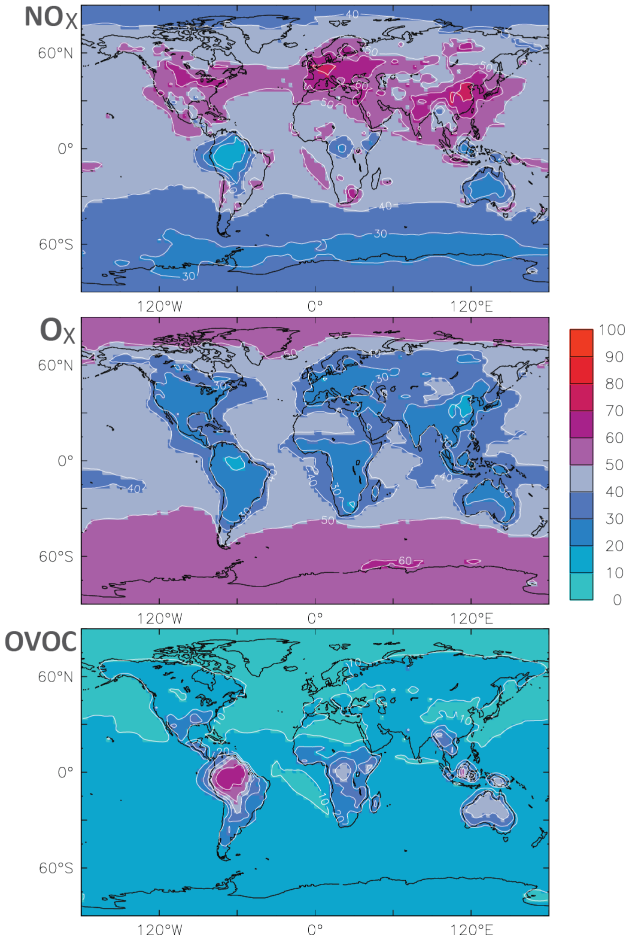

Figure 10: Fractional contributions to the OH recycling probability (% of *r*) in the troposphere by the NO_X (top), O_X (middle) and OVOC (bottom) mechanisms (sum of 3 panels is 100%).